frontiers | Frontiers in Energy Research

TYPE Original Research
PUBLISHED 20 February 2023
DOI 10.3389/fenrg.2023.1119090

OPEN ACCESS

EDITED BY
Antonio Moran,
Universidad de León, Spain

REVIEWED BY
Sunil A. Patil,
Indian Institute of Science Education and Research Mohali, India
Suman Bajracharya,
Luleå University of Technology, Sweden

*CORRESPONDENCE
Sven Kerzenmacher,
kerzenmacher@uni-bremen.de

SPECIALTY SECTION
This article was submitted to Fuel Cells, Electrolyzers and Membrane Reactors, a section of the journal Frontiers in Energy Research

RECEIVED 08 December 2022
ACCEPTED 06 February 2023
PUBLISHED 20 February 2023

CITATION
Vázquez I, Kerzenmacher S and Santiago Ó (2023), Stainless steel wool as novel bioanode for microbial electrolysis cells: A systematic study of materials. *Front. Energy Res.* 11:1119090. doi: 10.3389/fenrg.2023.1119090

Stainless steel wool as novel bioanode for microbial electrolysis cells: A systematic study of materials

Isaac Vázquez , Sven Kerzenmacher * and Óscar Santiago

Center for Environmental Research and Sustainable Technology (UFT), University of Bremen, Bremen, Germany

In the last years, microbial electrochemical technologies have received increasing attention due to their promising environmental potential. However, the identification of the most suitable materials for further development of these technologies tends to be challenging, especially for operation under realistic wastewater conditions. The objective of the present work is to carry out a systematic comparison of six anode materials (stainless-steel wool, carbon paper, graphite felt, graphite plate, graphite foil, and stainless-steel mesh) for microbial electrolysis cells operated for the treatment of brewery wastewater and determine the best material of these in sight of its electrochemical performance. For this purpose, the medium was semisynthetic brewery wastewater of low buffer capacity and low conductivity. The results suggest, that the degree of fermentation and characteristics of the studied media have only a minor impact on the limiting current density of the bioanodes. Here, the limiting current density of microbial anodes with stainless-steel wool (0.45 ± 0.07 $mA{\cdot}cm^{-2}$), a not so extensively studied promising material, outperformed commonly used materials such as graphite felt, without evidence of corrosion.

KEYWORDS

bioanode, stainless-steel wool, material comparison and selection, polarization curves (PC), brewery waste water

1 Introduction

A microbial electrolysis cell (MEC) is a device that could help in the wastewater treatment by consuming part of the chemical oxygen demand (COD) in the effluent while producing energy carriers such as hydrogen (Liu et al., 2005; Rozendal and Buisman, 2005; Rivera et al., 2018). In this process, anode respiring bacteria (ARB) metabolize organic carbon compounds and then deliver electrons onto a solid anode surface that acts as an external electron acceptor, while releasing carbonate and protons to the medium (Rozendal et al., 2006). The anode material with the ARB can also be referred to as bioanode. An external power source applies the necessary driving force to transport the electrons donated by the bacteria from the anode to the cathode surface, where hydrogen evolution takes place. The bioanode plays a key role in the operation of an MEC because it must not only collect the electrons produced by bacteria but also allow for the settling of bacterial communities in the form of a biofilm. In general, an ideal bioanode material would exhibit good biocompatibility, high electrical conductivity, large surface area, corrosion resistance, suitable mechanical strength, and toughness (Sonawane et al., 2018). Likewise,

properties such as long-term stability and robustness would be desirable for the scaling up of this technology (Rousseau et al., 2020).

Since the rise of microbial electrochemical technologies, numerous bioanode materials have been tested, whose results have been compiled and compared in book chapters (Dumitru and Scott, 2016; Kerzenmacher, 2019) and review papers (Sonawane et al., 2017; Yaqoob et al., 2021) alongside with their testing conditions. Some of the preferred materials have been carbon-based because of carbon abundance, low cost, biocompatibility, chemical and thermal stability (Dumitru and Scott, 2016; Fan et al., 2021); other metallic materials such as stainless-steel have also been tested previously showing promising results in terms of current density owing to their lower resistance and good microorganism adhesion (Pocaznoi et al., 2012). Also, stainless-steel wool of an unspecified alloy was already studied and compared against its polyaniline and polypyrrole-coated analogues (Sonawane et al., 2018), and stainless-steel fiber felt AISI 316L (EN 1.4404) has also been tested with various coatings (Hou et al., 2014). However, the current densities reported range widely for a same material tested by different research groups for their specific application and the ever-improving cultivation techniques. For instance, early experiments using graphite felt with pure *Geobacter sulfurreducens* got current densities of 0.03 $mA{\cdot}cm^{-2}$ to 0.11 $mA{\cdot}cm^{-2}$ in 10 mM acetate medium (Bond and Lovley, 2003), later experiments reached current densities of 0.76 $mA{\cdot}cm^{-2}$ in 15 mM acetate medium (Kipf et al., 2018) and 1.2 $mA{\cdot}cm^{-2}$ in 48 mM acetate medium (Adachi et al., 2010). Furthermore, the same research group that obtained 0.76 $mA{\cdot}cm^{-2}$ with graphite felt using *G. sulfurreducens* in 15 mM acetate medium achieved 0.05 $mA{\cdot}cm^{-2}$ using *Shewanella oneidensis* in 50 mM DL-Lactate medium (Kipf et al., 2013). Due to differences in experimental conditions between studies such as cultivation temperature or potential, the inoculum, the substrate, the duration of the analysis, the history of the experiment or the criteria for comparison, it becomes difficult to compare the performance of the materials and to ascertain the most suitable from a scientific and engineering approach.

However, not only the diverse experimental conditions contribute to the comparison difficulties, but also the complexity of the medium that the anodes are studied in. The characterization of microbial anode materials in real complex effluents such as brewery wastewater poses a difficulty as the effluent contains fermentative bacteria, creating reactor microbiomes which could degrade variably the wastewater, causing changes in the pH, amount and type of organic compounds available for the ARB and making difficult to keep constant reactor conditions (Koch et al., 2019; Álvarez Esquivel et al., 2020). Thus, a comparison method between materials is needed and it should account for the changes in media, as well as ensuring reproducible and highly electroactive biofilms through independent replicate reactors.

Addressing the hurdles above mentioned, the objective of this work is to compare four carbon-based materials (graphite plate, graphite foil, graphite felt, and carbon paper) and two metallic ones (stainless-steel wool and stainless-steel mesh) and to identify the anode material with the best electrochemical performance. In this sense, the performance of the stainless-steel wool in relation to its packing density is further analyzed because of its outstanding performance. Additionally, the influence of the fermentation degree of the wastewater in the electrochemical performance of the bioanodes is evaluated.

For this purpose, all the explored anodes undergo the same experimental procedure. Also, the experiments are done under the same changing-media conditions and focusing in their polarization behavior to minimize longer term variations of the media usually seen in chronoamperometric experiments in poorly-buffered low-conductivity media. To account for the fermentative process in the wastewater, the assessment of anodes considers three types of semisynthetic brewery wastewater media: a fresh, a prefermented, and an aged one. That way, that the performance of the anodes is evaluated in wastewater with different degrees of fermentation and repeating the same procedure four times to obtain independent quadruplicates.

2 Materials and methods

All the chemicals used for the preparation of media were from Carl Roth, Germany. Deionized water for the media had a resistivity greater than 18 MΩ·cm. A purge gas mixture consisting of 20% mol CO_2 (purity ≥ 99.995%, Linde, Germany) and 80% mol N_2 (purity ≥ 99.999%, Air Liquide, Germany) was used for anaerobization. For filtration procedures 0.2 µm surfactant-free cellulose acetate filters were used (Sartorius, Germany). Kits from Hach-Lange, Germany, were used to measure the COD (Cuvettes LCK014, LCK514) and organic acids (Cuvettes LCK365) with the help of the detector DR 3900, which also was used to measure optical density at 600 nm (OD_{600}). For pH and conductivity measurements, offline sampling was done with the help of WTW TetraCon 325 and SenTix Mic, probes respectively, connected to Multiline P4 measurement devices (all of them from Xylem Analytics Germany GmbH).

All the potentials throughout this work are referred to a saturated calomel electrode (SCE, 241 mV vs. standard hydrogen electrode, model KE11, Xylem Analytics Germany GmbH, Germany). The measuring of current intensity and control of the potential applied to the working electrodes were done with a multichannel potentiostat-galvanostat systems (PGU-MOD 500mA-4K, IPS Elektroniklabor GmbH and Co., KG, Germany).

2.1 Inoculum

A first source of anode respiring bacteria for the reactor was *G. sulfurreducens* PCA enriched in an anaerobic medium (Coppi et al., 2001) during 48 h. The cells went through a centrifugation and washing process three times to remove the soluble electron acceptors prior to their inoculation at an OD_{600} of 0.060 as described elsewhere (Kipf et al., 2014). In this work the salts solution described in Section 2.2 was used for the washing process. The second source of microorganisms was real wastewater from the effluent of a local brewery inoculated at 1% V/V in order to provide bacteria capable of breaking down complex organic compounds naturally occurring in the stream. Indeed, the simultaneous use of two inocula was to provide an acetogenic community (from brewery wastewater-occurring bacteria) and electrogenic bacteria (*G. sulfurreducens*). This way a bacterial consortium capable of degrading some COD typically occurring in brewery wastewater streams down through an

TABLE 1 Materials under study for biofilm support.

Material	Type	Thickness	Manufacturer
Graphite plate	MR40	3 mm	Müller and Rossner GmbH and Co., KG, Troisdorf, Germany
Carbon paper	H2315	0.210 mm (at 0.025 MPa)	Freudenberg Performance Materials SE and Co., KG, Weinheim, Germany
Graphite foil	10832	0.254 mm	Thermo Fischer (Kandel) GmbH, Kandel, Germany
Graphite felt	GFD 2.5 EA	2.5 mm (nominal)	SGL Carbon SE, Wiesbaden, Germany
Stainless-steel wool	EN 1.4113 Medium ($d_{wire} \approx 0.090$ mm)	3 mm approx	RAKSO, Oscar Weil GmbH, Lahr, Germany
Stainless-steel mesh	EN 1.4301 $w = 0.224$ mm $d = 0.100$ mm	0.448 mm approx. (based on wire diameter)	Haver and Boecker OHG, Oelde, Germany

electrogenic pathway is provided in order to compare all the anode materials under the same conditions.

2.2 Semisynthetic brewery wastewater medium

For the reactor medium to resemble the total bound nitrogen (~65 mg·L^{-1}) and orthophosphate as phosphorous (~36 mg·L^{-1}) of real brewery wastewater, a salts solution was used as basis for all semisynthetic brewery wastewater (SBW) media, which contained 0.745 g $NaHCO_3$, 0.196 g K_2HPO_4, 0.315 g $(NH_4)_2SO_4$ and 0.105 g NaCl and deionized water per liter of salts solution. The fresh semisynthetic brewery wastewater medium (SBW-fresh) contained additionally 15.2 mL of sterile filtered local pilsner beer per liter of autoclaved anaerobic salts solution. To prepare the prefermented medium (SBW-prefermented), 1 L SBW-fresh got additionally 10 mL of real wastewater and stayed 2 days under incubation in a Schott bottle at 30°C with a magnetic stirrer at 300 rpm with steady CO_2/N_2 gas-mix purging. Only for the startup phase of the electrochemical reactor, prior to inoculation and cultivation procedures, the medium was complemented with 2 mL of 10% m/V yeast extract per liter of medium.

2.3 Experimental setup and material comparison

A sample of each of the six electrode materials was placed in every independent quadruplicate of the experiments. These anode comparison experiments were carried out in a previously described battery glass reactor (Erben et al., 2021) under constant purging with CO_2/N_2 gas-mix mixture throughout the experiment (a schematic is provided in Supplementary Figure S1). The anaerobization of all media and reactors was started 24 h prior to the experiments after autoclaving the reactors and gassing through 0.2 µm sterile filters. The specifications of the electrodes under study are shown on Table 1. A square-shaped electrode of each material with a projected surface area of 2.25 cm^2 was sonicated in 70% V/V isopropanol for 20 min and then in deionized water for 10 min three consecutive times. Then the electrodes were placed in square-shaped electrode holders made of polypropylene with only one side exposed to the bulk of the reactor medium and a silicone gasket isolating the back side of the electrode from the medium. On that non-exposed side of the anode, a polypropylene frame held a titanium wire (99.7 %wt., 0.25 mm diameter, Sigma Aldrich, United States of America) used as current collector. Platinum mesh electrodes (99.9 %wt., 0.06 mm wire diameter, 0.25 mm nominal aperture, Goodfellow, Germany) were placed as counter electrodes on the back side of the anode, away from the electric field lines between the reference electrode in the center of the reactor and the anodes.

2.4 Experimental procedure and reactor operation

A graphic representation of the course of the 28-day experiment is shown in Figure 1. During the first 24 h the reactor was operated in chronoamperometric mode polarizing the electrodes at 151 mV vs. SCE, the next 5 days the electrodes were polarized at −241 mV vs. SCE. The two different potentials applied were to ensure bacteria adhesion and growth (151 mV vs. SCE, equivalent to 200 mV vs. Ag/AgCl) and to maintain the biofilm with current production at lower overall cell voltage (−241 mV vs. SCE, equivalent to −200 mV vs. Ag/AgCl), which are potentials that have been previously used (Kipf et al., 2018; Riedl et al., 2019).On day 7, a polarization curve was acquired for each electrode in the medium that had been inside of the reactor for the past days (also called "aged" semisynthetic brewery wastewater, SBW-aged). For this purpose, the electrodes were left for 1 h at open circuit potential and then the potential was increased from −400 mV vs. SCE to 0 mV vs. SCE in steps of 50 mV every 30 min. Subsequently, the electrodes inside the reactor were polarized again to −241 mV vs. SCE overnight. On day 8 the whole medium inside the reactor was exchanged for SBW-prefermented with a GP1000 peristaltic pump (Thermo Fischer, Germany). During the medium exchange the potentiostats were turned off to avoid damaging the biofilm and the purging gas flowrate was tripled to prevent oxygen ingress into the reactor. The media exchanges did not last longer than 10 min. Immediately after that, the reactor was equilibrated for 1 h at −241 mV vs. SCE and the polarization curve acquisition was started from the open circuit potential in the same manner as in the previous day. On the next day the medium was exchanged to SBW-fresh to get the polarization

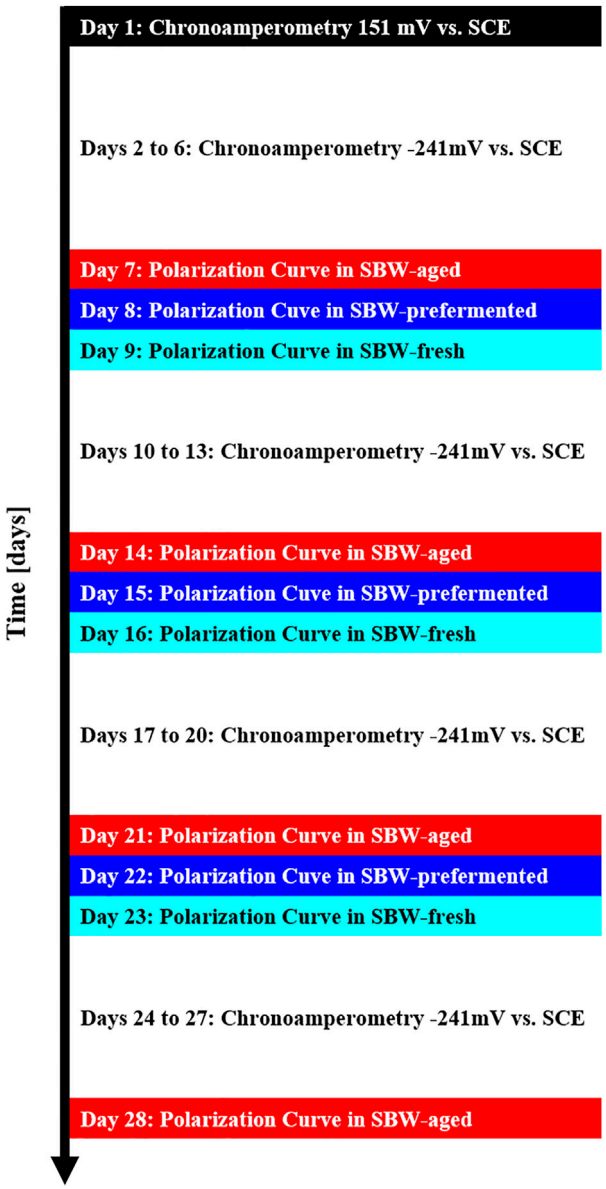

FIGURE 1
Course of the experiment with the sequence of polarization experiments done on the bioanodes. Chronoamperometric measurements are interrupted for polarization curve studies carried out in various media from −400 mV vs. SCE to 0 mV vs. SCE in 50 mV steps for 30 min, followed by cyclic voltammetries from −600 mV vs. SCE to 100 mV vs. SCE at a scan rate of 5 mV·s^{-1}.

curve and the same medium stayed in the reactor for the following 4 days so to become SBW-aged. The polarization curves were obtained each week for the next 2 weeks following the same procedure including the media exchanges, as shown in Figure 1. Before taking the reactor out of operation, a last polarization curve in the aged medium was obtained.

It should be noted that in this work the chronoamperometry studies were used as an operation to keep the biofilm living between the polarization curves and the chronoamperometry operation was kept around 5 days to prevent fermenting bacteria from outnumbering electrogenic bacteria. During this time, the fresh medium (SBW-fresh) undergoes a fermentation process in the reactor (it becomes SBW-aged). Also, the reactor ran with a prefermented medium (SBW-prefermented) during a short period of time because the prefermented medium serves as a standardized baseline for comparison of polarization curves in aged and fresh medium.

After termination of every polarization curve, cyclic voltammetries from −600 mV vs. SCE to 100 mV vs. SCE at a scan rate of 5 mV·s^{-1} were conducted but the results were not used during this analysis. Also, at that point the uncompensated resistance of the medium was measured too with the help of an Interface 1010T potentiostat (Gamry Instruments, Germany). However, this data was not reliable and was therefore not used for the correction of the anode potentials. Instead, to account for the low conductivity of the medium the polarization curves were corrected (also known as IR_u-drop compensation) following the same strategy previously reported, which had considered the conductivity as well as the geometry and distances of the electrodes (Madjarov et al., 2017). For this work the potential is corrected using Eq. 1.

$$E_{calc} = E_{app} - \frac{K_R I}{\sigma} \quad (1)$$

where E_{calc} is the corrected applied potential on the electrode versus the reference electrode, E_{app} is the applied potential by the potentiostat without correction, I is the current intensity yielded by the bioanode, K_R is the geometry factor of the reactor (for this design is 38.67 m^{-1}, calculated following the work of Madjarov et al., 2017) accounting for the position of the bioanode with respect to the reference electrode and σ is the conductivity of the medium measured at the beginning of each polarization curve experiment.

Every day the COD (Hach-Lange cuvettes LCK014, LCK514), organic acids content (Hach-Lange cuvette LCK365), OD_{600} (Hach-Lange spectrophotometer DR 3900), pH and conductivity were monitored to ensure stable operation of the reactor. These parameters were also checked before and after the polarization curve studies. The parameters of the reactor evolved freely, but the pH was corrected manually with 1.0 M NaOH if lower than 6.4.

2.5 Corrosion analysis

The metallic materials underwent further corrosion studies under abiotic conditions as done by previous authors (Baudler et al., 2015). For this purpose, two studies were carried out. The first experiment was a linear-sweep voltammetry (LSV) between −600 mV vs. SCE and 500 mV vs. SCE at 1 mV·s^{-1} in a three-electrode setup (counter electrode graphite felt GFD 2.5 EA, SGL Carbon SE, Germany) inside a modified Schott bottle setup with SBW-fresh and with SBW-prefermented. The SBW-prefermented medium was twice-centrifuged to remove bacteria that could interfere with the corrosion measurement. The same medium was used for each electrode, but the electrodes were analyzed in separate half-cells to obtain independent triplicates. The corrosion was assessed based on the exchange current density for corrosion (j_{corr}) in a Tafel plot. The second experiment was a chronoamperometric operation corresponding to the first week of operation of the battery glass reactors operated with brewery

TABLE 2 Wastewater characteristics before and after the polarization curve experiments averaged over the four batches.

		pH	COD	Organic Acids	OD_{600}	Conductivity
		[-]	[mg $O_2 \cdot L^{-1}$]	[mg $Acetate_{eq} \cdot L^{-1}$]	[-]	[mS·cm^{-1}]
SBW-fresh	Start	6.64 ± 0.15	1940 ± 237	31 ± 6	0.000 ± 0.004	1.72 ± 0.02
	End	6.50 ± 0.13	1670 ± 83	236 ± 13	0.105 ± 0.053	1.69 ± 0.02
SBW-prefermented	Start	6.61 ± 0.24	1608 ± 95	212 ± 15	0.161 ± 0.017	1.69 ± 0.01
	End	6.62 ± 0.14	1608 ± 56	244 ± 21	0.138 ± 0.018	1.73 ± 0.02
SBW-aged	Start	6.75 ± 0.27	1391 ± 297	763 ± 257	0.130 ± 0.075	2.53 ± 0.35
	End	6.78 ± 0.29	1417 ± 280	750 ± 271	0.131 ± 0.076	2.53 ± 0.35

wastewater in presence of electroactive bacteria. However, in this case, the battery glass reactor was not inoculated but rather twice-centrifuged, twice-sterile-filtered SBW-prefermented was used. At the end of the week, a polarization curve was performed in the same manner as described in the previous section. The morphology of the electrodes used for corrosion experiments was studied with the help of a field emission scanning electron microscope (Zeiss Supra 40, Germany; acceleration potential of 3.0 kV), and compared against clean unused samples.

2.6 Determination of the influence of packing density of stainless-steel wool

Stainless-steel wool (made from alloy 1.4113 which has not previously been studied as bioanode), is flexible and its fibers can change the overall macroscopic porosity of the electrode depending on the packing density of the electrode, which in turn could impact on the available surface area for ARB colonization. Hence the same strategy described in Section 2.4 was followed in order to compare one-to-one stainless-steel wool electrodes of different packing density to determine its influence and to identify potentially beneficial packing densities. The electrodes were placed in the same electrode holders than the electrodes presented on Table 1 with 3 mm thickness and with masses: 0.137, 0.291, 0.407, 0.737, and 1.010 g. Having different masses in the same size electrode holders implies a change in the compression undergone by the electrodes. The results were assessed evaluating the sensitivity of the limiting current density, the specific current per unit mass, the slope of the anode polarization curve and the open circuit potential against the changes in the mass of the electrodes.

3 Results and discussion

The chronoamperometric cultivation and monitoring of the bioanodes as well as their polarization curves yield insight on two major criteria for the study and selection of anode materials, respectively: on one hand the long-term stability of the attainable current density by the anode materials and the reproducibility of such current densities; on the other hand, the achievable current density by the bioanodes at various potentials, especially their limiting current density (j_{lim}). To better understand the value of each experiment, the results are presented separately. In addition to that, Table 2 presents a summary of the measured physical and chemical parameters of the wastewater media used in this work. The parameters were averaged over the four batches at the beginning and the end of each polarization curve.

3.1 Chronoamperometry

The average current densities obtained with the different bioanodes throughout the experiment are presented in Figure 2 (error bars accounting for the variability of the independent quadruplicate experiments). Due to the low conductivity of the medium (and the associated high uncompensated resistance), the actual anode potentials of electrodes with high current density where significantly lower than the set potential. In such cases, the achievable current density at the set potential is actually underestimated. Further information on the corrected electrode potentials (based on the uncompensated resistance) can be found in Supplementary Figure S2.

During the first 24 h at 151 mV vs. SCE, the porous carbon-based materials (carbon paper and graphite felt) produce the highest current density. When the anode potential is decreased to −241 mV vs. SCE, the steady increase in current density of all materials is kept, but two phenomena can be identified. One is that stainless-steel wool current density production rises higher than all the other materials tested and the second is that stainless-steel mesh start producing appreciable current density.

It is also noticeable that approximately 1.8–1.9 days after the start of the experiment all current densities decrease drastically, due to the acidification of the medium, characterized by a pH drop to values in the range of 4.95–5.73 associated with fermentation. A similar trend is observed approximately 24 h after resuming the chronoamperometry after the interruptions due to the polarization curve measurements on weeks 2, 3, and 4. The current densities rise back as the pH stabilizes around 6.7 (see Table 2, SBW-aged) due to repeated pH corrections with NaOH. These corrections happened regularly throughout the experiment and are not shown in Figure 2. Generally, all the anodes show an increasing current density in the first week, but on the following weeks the trends change drastically. Whereas the current density of the stainless-steel wool rises

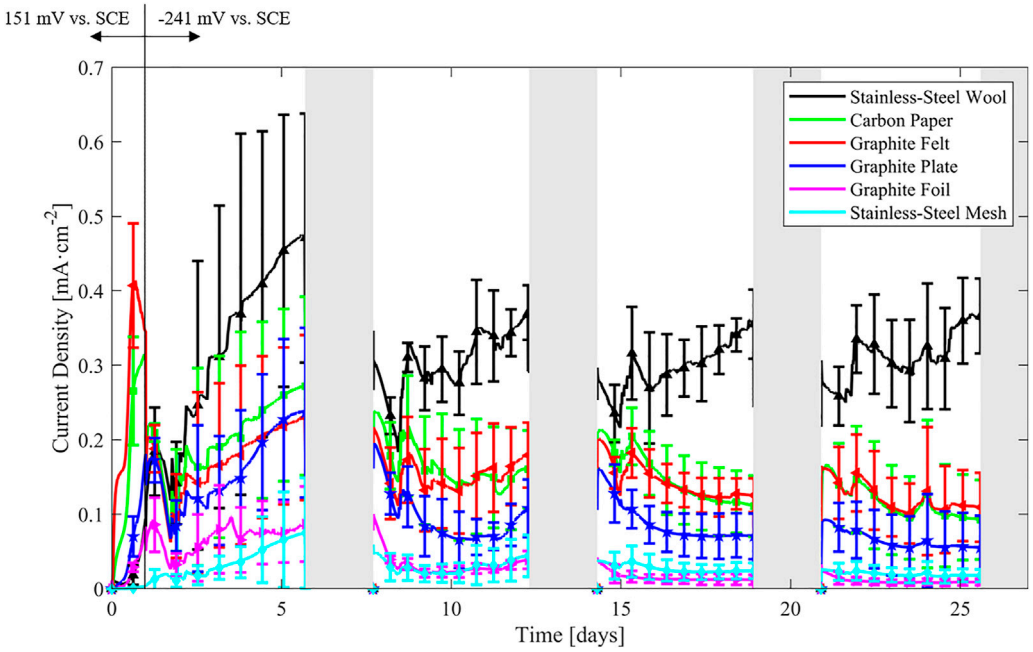

FIGURE 2
Current densities during chronoamperometric operation obtained in independent quadruplicate experiments. On the first day, the electrodes were polarized at 151 mV vs. SCE and −241 mV vs. SCE on the following days. Shaded regions indicate the interruptions for polarization curves.

gradually approaching 0.36 ± 0.05 mA·cm^{-2} towards the end of weeks 2–4, the other materials tend to show a steadily decreasing current density. This is more noticeable on the third and fourth weeks.

Due to batch to batch variations, the error bars of the chronoamperometries tend to show some degree of overlapping. Towards the third and fourth weeks the error bars tend to narrow down and the higher current density of stainless-steel wool becomes clearer under the described experimental conditions. Thus, the materials could be set in four groups in terms of current density, even after considering the variation of the quadruplicates: 1) stainless-steel wool, 2) graphite felt and carbon paper, 3) graphite plate, and 4) stainless-steel mesh and graphite foil. Another grouping could consider the three-dimensional materials (stainless-steel wool, graphite felt and carbon paper) with higher current densities than non-porous materials (graphite plate, graphite foil and stainless-steel mesh) with lower current densities.

3.2 Polarization curve

Three polarization curves in SBW-fresh and SBW-prefermented and four polarization curves in SBW-aged were obtained for the six different anode materials. These curves were corrected for uncompensated resistance as stated in Section 2.4. Selected parameters of the polarization curves are presented in Figures 3–5. These plots show the limiting current density (defined in our experiments as the highest current density achieved during the polarization curve), slope of the ohmic region of the bioanodes, and open circuit potential of the polarization curves. The actual polarization curves for the anode materials and media are available in the Supplementary Information (Supplementary Figures S3–S5).

In general, the observed limiting current densities in SBW-aged were systematically lower than the current densities obtained in SBW-fresh or SBW-prefermented over the weeks, but the system did not seem to show higher current densities upon prefermentation of the medium, despite the fact that the organic acids content was higher (Table 2). Another notorious feature is the higher limiting current density of stainless-steel wool bioanodes than the others and its stability over time (Figure 3A). Bioanodes with carbon paper and graphite felt show the second highest limiting current densities at the beginning of the experiment but decrease fast over the weeks. A similar trend is observed for graphite plate, but it remains slightly lower than its paper and felt counterparts. Graphite foil and stainless-steel mesh do not seem to allow high limiting current densities, still they tend to go lower over time under the described experimental conditions. This trend is in good agreement with that observed throughout the chronoamperometric experiment and points towards stainless-steel wool being a suitable material for bioanodes in terms of high current density and robustness.

The slope of the polarization curves in the ohmic region shown on Figure 4 varies from around 0.05 kΩ·cm^2 to almost 20 kΩ·cm^2 implying that all the bioanodes have very different internal resistances. The trend of the slopes follows an inverse fashion to that of the limiting current density, as resistance seems to increase over the course of the experiment, which might be related either to a decrease of the conductivity of the biofilm and its viability (Dhar et al., 2017), with an overgrowth of the biofilm on the porous structure of the biofilm (Baudler et al., 2017) or with the formation of a low-conductive passivated layer on the metallic electrode

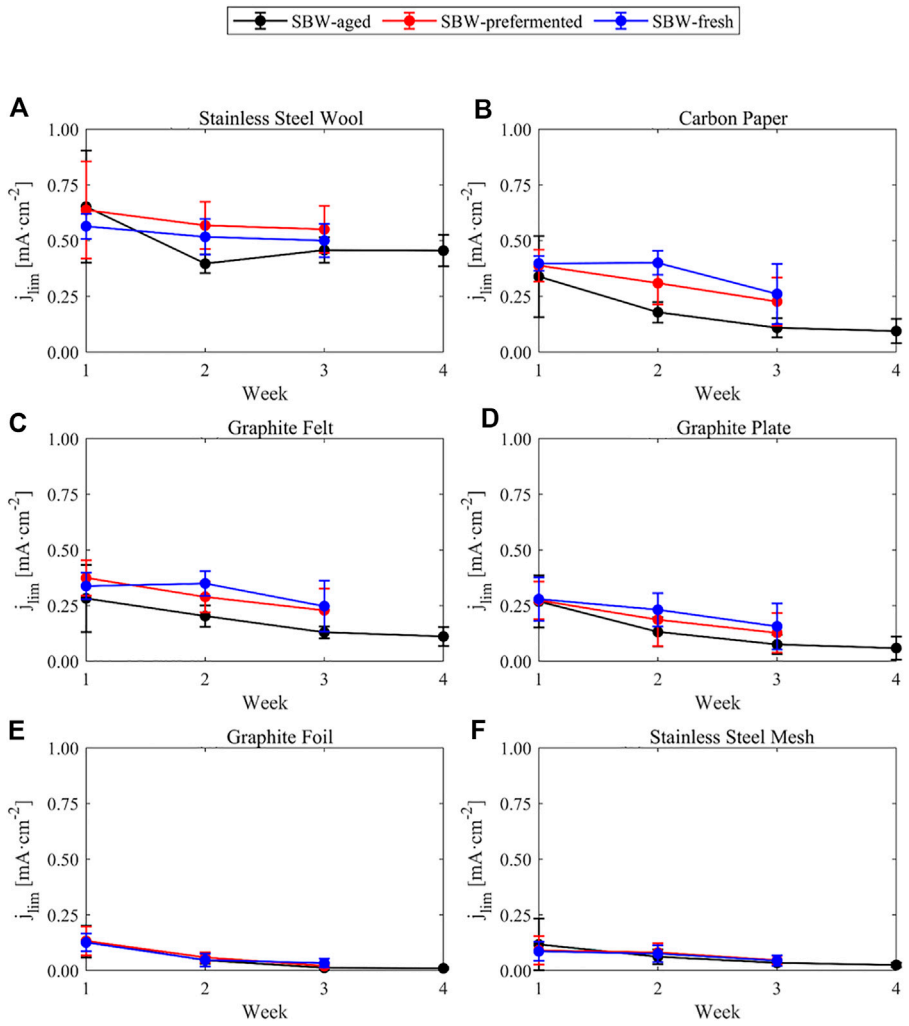

FIGURE 3
Limiting current density (j_{lim}) of the bioanodes throughout the weeks of the experiment and bound with lines for visual aid. Data series were tested in SBW media with different degrees of fermentation. **(A)** Stainless-steel wool **(B)** Carbon paper **(C)** Graphite felt **(D)** Graphite plate **(E)** Graphite foil **(F)** Stainless-steel mesh.

surfaces (Dumas et al., 2008; Kipf et al., 2013). In stainless-steel wool the increase of resistance is asymptotic and at all times lower than the other materials, making it an interesting material for longer term operation.

The open circuit potential of most of the bioanodes, except graphite foil, remains statistically constant over the weeks (Figure 5). It coincides with the potential of the internal redox carrier of other biofilms dominated by *G. sulfurreducens* and close to the standard redox potential of the $FAD/FADH_2$ (around −461 mV vs. SCE) (Thauer et al., 1977; Riedl et al., 2019) or with the *c*-type cytochrome OmcZ (between −447 mV vs. SCE and −475 mV vs. SCE) (Inoue et al., 2010). The closeness of the open circuit potential to the redox carriers of known *G. sulfurreducens* biofilms could be used as evidence to the presence of *G. sulfurreducens*. However, the in-depth analysis of the open circuit potential in relation to specific redox carriers goes beyond the scope of this work.

In general, it can be seen that most electrodes decrease their limiting current density (Figure 3) and increase their resistance over time (Figure 4) in a steady fashion, except from stainless-steel wool, whose limiting current density and resistance does not show significant changes from week 2 on.

The overall duration of each reactor run was 28 days. During this time the media in the reactors underwent compositional changes, while the COD and pH of the fresh and prefermented media fed in to the reactors was kept constant. The main physical and chemical characteristics of the media before and after the polarization curves are reported on Table 2, thus enabling the detection of potentially significant changes within the reactor, especially during the polarization curve experiments. SBW-fresh showed an increase in the organic acids, optical density, and organic acids, after recording the polarization curves implying a fast-fermentative process.

SBW-prefermented showed a slight decrease in the optical density and a slight rise in the conductivity, possibly due to the death of biomass and resuspension of cell debris and ions from the previous media. In spite of that, at the end point of the polarization curve recording, the characteristics of the fresh and prefermented medium are comparable, due to the time demand of polarization

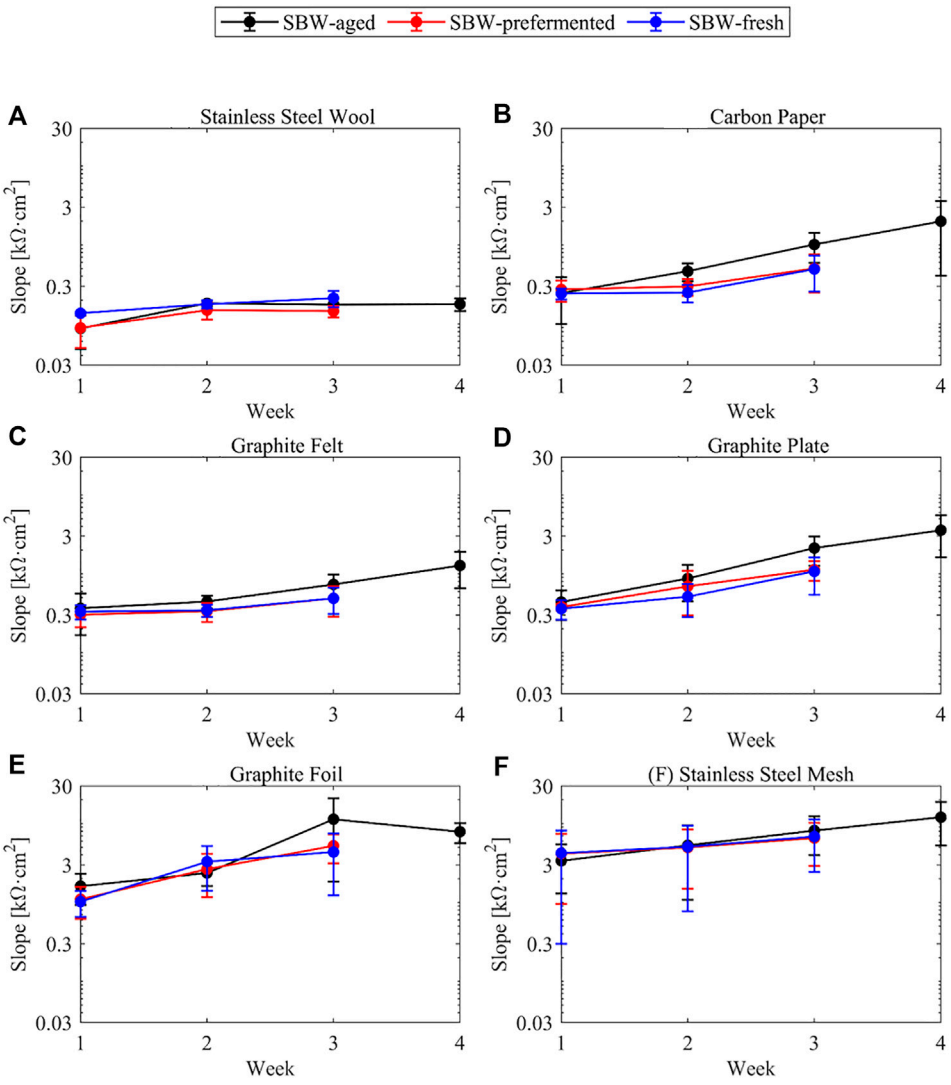

FIGURE 4
Slope of the bioanodes in the ohmic region throughout the weeks of the experiment in logarithmic scale and bound with lines for visual aid. **(A)** Stainless-steel wool **(B)** Carbon paper **(C)** Graphite felt **(D)** Graphite plate **(E)** Graphite foil **(F)** Stainless-steel mesh.

curve recording (see row "End" of SBW-fresh in Table 2). Thus, in our case we can draw no conclusion on the effect of fermentation degree on the limiting current density.

SBW-aged did not show appreciable changes in the media during performing polarization curve measurements, but a high variability of parameters such as the organic acids in the medium between the different batches (see standard deviation of the aged media characteristics in Table 2). However, the limiting current densities in aged medium show only little difference to the values obtained in fresh or prefermented medium. Furthermore, despite the large standard deviation in aged medium characteristics don not lead to a high standard deviation of the limiting current densities. This suggest, that the characteristics of the investigated media play a minor role on the electrochemical performance of the bioanodes.

The simultaneous polarization curve analysis of all anodes allows a fair comparison of the bioanode performance under the same described medium conditions, thus addressing the previously described comparability problems among authors and anode media. Also, the inoculation procedure ensured the fast startup of the systems while getting consistent data across trials. In this work the highest limiting current density is obtained on the week 1 with stainless-steel wool (0.64 ± 0.22 mA·cm^{-2} at −281 ± 72 mV vs. SCE) at a comparable level to the values obtained in a previous work using activated carbon cloth (0.77 ± 0.06 mA·cm^{-2} at −275 ± 12 mV vs. SCE) using a pure culture of *G. sulfurreducens* in a well-buffered medium and using acetate as sole electron acceptor (Kipf et al., 2018). Stainless-steel wool performed so well even on the week 4 that the current density of 0.42 ± 0.06 mA·cm^{-2} at −359 ± 17 mV vs. SCE outperforms materials such as titanium and stainless steel in the aforementioned study with pure culture in buffered medium and still provided 54% of the activated carbon cloth current (Kipf et al., 2018).

In summary, the chronoamperometry and polarization curve experiments performed in this work at our experimental conditions determined EN 1.4113 stainless-steel wool to be the best performing material of all six. Some hypotheses might be the large surface area of the material, the higher conductivity of the metallic material in

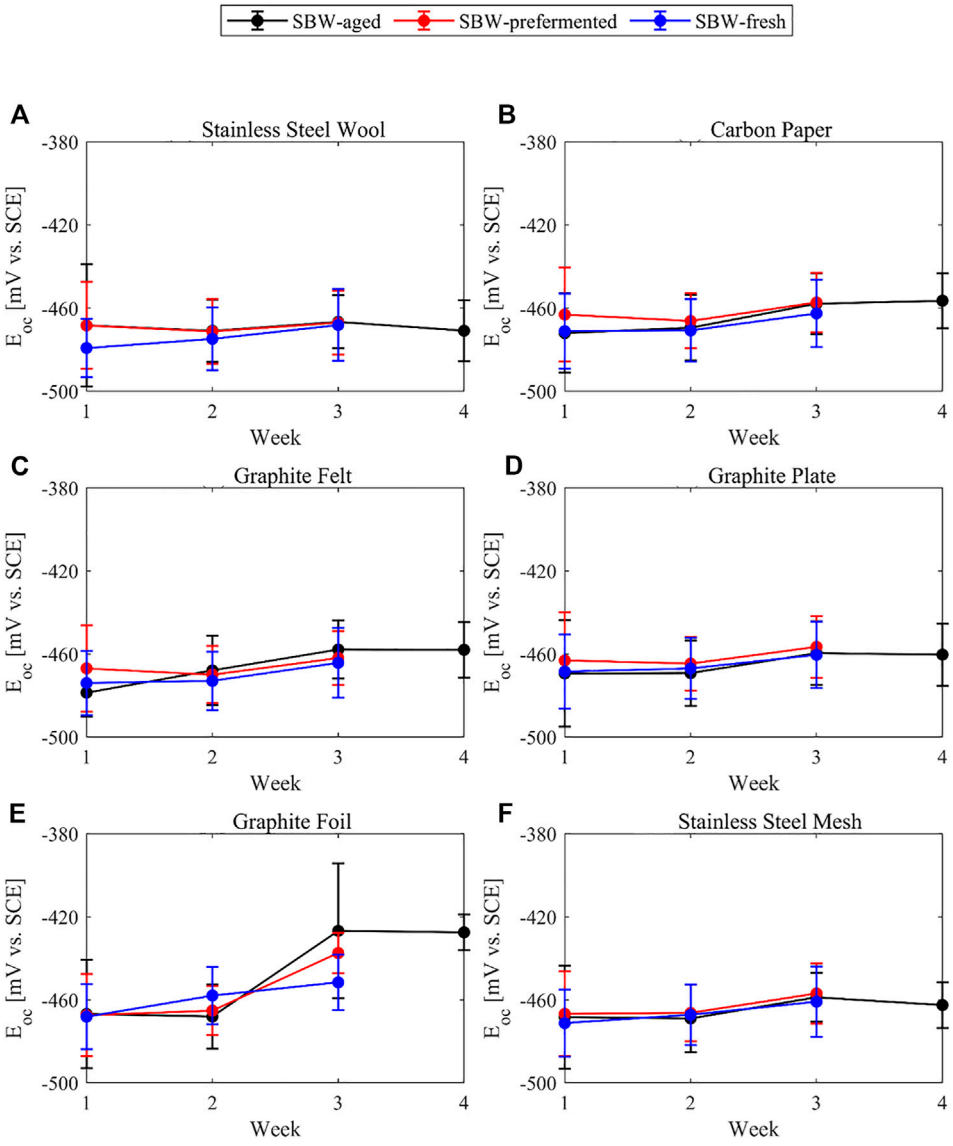

FIGURE 5
Open circuit potential of the bioanodes against the reference electrode over the weeks of the experiment and bound with lines for visual aid. **(A)** Stainless-steel wool **(B)** Carbon paper **(C)** Graphite felt **(D)** Graphite plate **(E)** Graphite foil **(F)** Stainless-steel mesh.

comparison to graphitic materials or the absence of nickel in the alloy used. Also, in the following sections the corrosion behavior and influence of packing density are further analyzed.

3.3 Corrosion evaluation of the metallic anodes

The first experiment for the evaluation of corrosion was the LSV. The metallic anodes did not show evidence of active corrosion in LSV experiments (Figure 6). While scanning along the potential range at 1 $mV{\cdot}s^{-1}$, the current densities observed at −241 mV vs. SCE did not exceed 5% of the current density seen in experiments in the presence of ARB on the electrode surface (further data values on Supplementary Table S1). The second experiment for the evaluation of corrosion was the abiotic chronoamperometry followed by polarization curve acquisition, which is a longer-term experiment than the LSV scans. The abiotic polarization curves (Supplementary Figure S6) in quasi-static conditions showed about two orders of magnitude lower current densities than biotic experiments. However, after SEM inspection (Figure 7), stainless-steel mesh did show morphological changes on the surface of the electrode (see the black craters with white borders in Figure 7D), similar to a pitting corrosion process, which could not be confirmed through electrochemical techniques. On the contrary, the stainless-steel wool did not show appreciable changes in the surface morphology at the analyzed conditions. One of the main chemical differences between both electrode materials is that the stainless-steel mesh alloy (EN 1.4301) contains nickel as opposed to the stainless-steel wool alloy (EN 1.4113). Previous works had compared stainless steel EN 1.4301 (8 %wt., to 10.5 %wt., nickel) against nickel as anode material showing lower current densities in nickel than in stainless

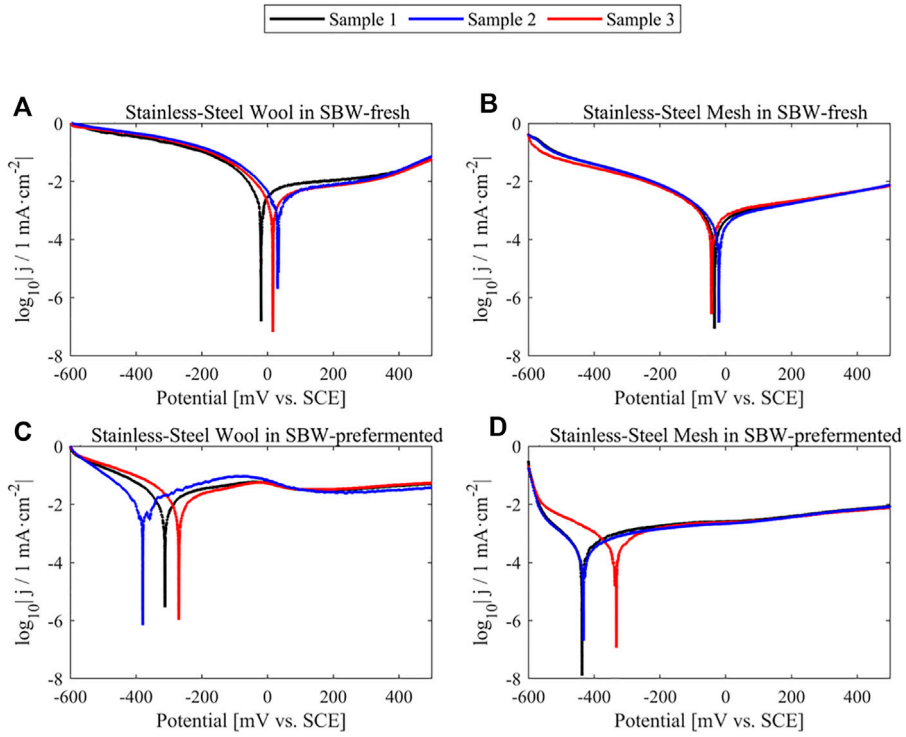

FIGURE 6
Triplicate linear-sweep voltammetries of clean metallic anode materials in abiotic conditions, shown in logarithmic representation for graphical Tafel parameter determination. **(A)** Stainless-steel wool in medium SBW-fresh **(B)** Stainless-steel mesh in medium SBW-fresh **(C)** Stainless-steel wool in medium SBW-prefermented **(D)** Stainless-steel mesh in medium SBW-preferemented.

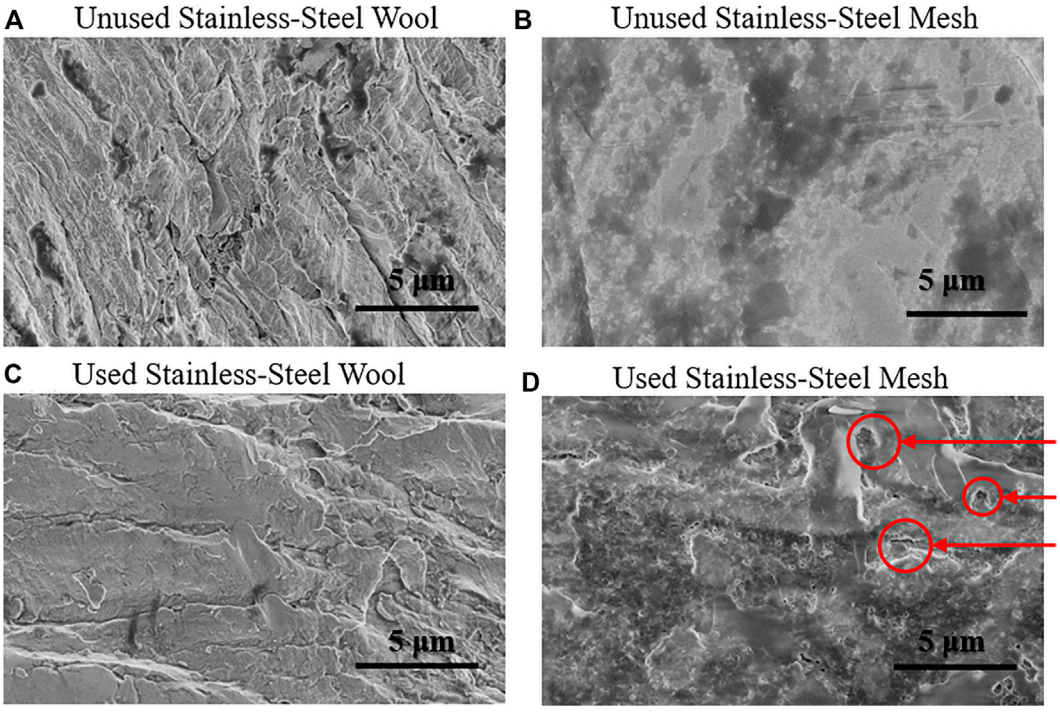

FIGURE 7
Scanning electron micrographs of metallic anode materials. **(A)** Unused stainless-steel wool **(B)** Unused stainless-steel mesh **(C)** Used stainless-steel wool **(D)** Used stainless-steel mesh. Arrows in **(D)** indicated the morphological changes (black craters with white borders) similar to pitting as compared to **(B)**.

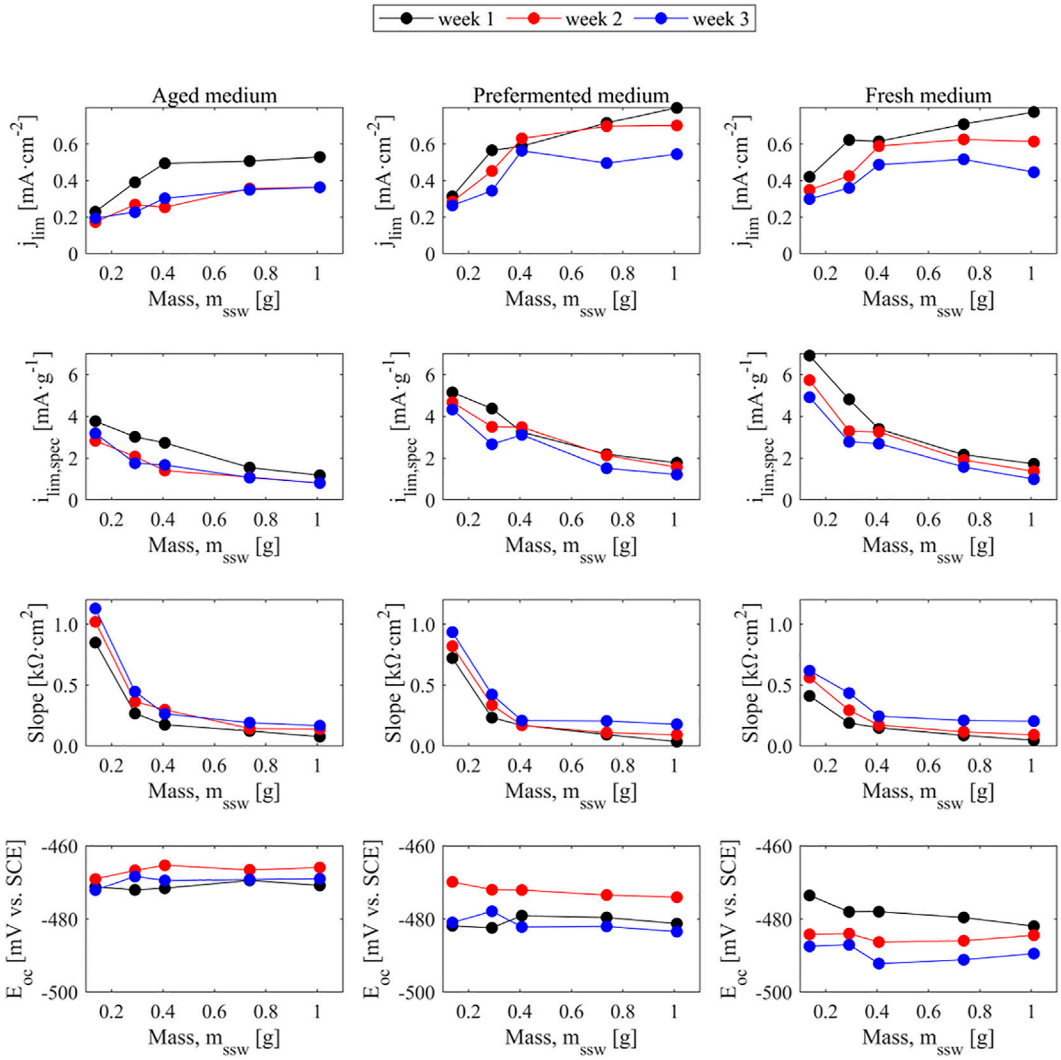

FIGURE 8
Limiting current density, limiting specific current referred to the mass of the electrodes, slope and open circuit potential of stainless-steel wool bioanodes against the mass of the electrodes. Straight binding lines are mere visual aids.

steel, yet both materials yielded lower current densities than graphite-based materials, possibly due to microorganism interactions with nickel-containing electrodes (Baudler et al., 2015). In the present study stainless-steel wool, made of a nickel-free stainless-steel alloy (EN 1.4113), seems to outperform graphite-based materials with negligible corrosive current contributions.

3.4 Effect of stainless-steel wool packing density on electrode performance

Stainless-steel wool gave the most promising results based on their polarization behavior, and it also offers the advantage of easily changing packing density upon compression, which in turn changes its surface area per volume. In this work the packing density was varied without modifying the thickness of the electrode. The modification of the surface area per volume feature may play a significant role in the electrochemical performance of an MEC for brewery wastewater treatment as higher packing degrees might change the current density or resistance of the bioanode. This can be seen in Figure 8, where the use of different packing densities (referred to the mass of stainless-steel wool inside the electrode frames) leads to specific currents ranging from 1 to 7 mA·g^{-1}. While higher amounts of stainless-steel wool help obtaining higher current densities, the specific utilization of the anode surface decrease either by availability of the surface for microorganisms or due to transport limitations to the innermost part of the anodes. Higher packing densities of stainless-steel wool improve the electrical connection between the wires, which is inferred from the flattening of the slope of the polarization curves as seen in the third row of Figure 8. The packing density did not seem to influence the open circuit potential of the bioanodes under these testing conditions. In sight of the tradeoff between the mass-specific current, the current density, and the anode resistance, a packing density of 603 mg·cm^{-3} (0.407 g of stainless-steel wool in the 15 mm × 15 mm × 3 mm electrode holder) is the most appropriate from the electrochemical perspective, which is the same degree of packing used in the experiments described in Section 2.4.

The polarization curves of the stainless-steel wool anodes at different packing densities can be found in the Supplementary Information (Supplementary Figures S7–S9).

4 Conclusion

Studying the materials in a simultaneous way through chronoamperometry methods and polarization curves as presented in the methodology is a reliable tool to determine the electrochemical performance of bioanode materials and comparing them, regardless of the ongoing fermentation process. Step-wise polarization curve experiments together with the use of semisynthetic media with set degrees of fermentation gave significant insight on the electrochemical performance of anode materials for brewery wastewater treatment applications. Here, the results suggest that the degree of fermentation and characteristics of the studied media have only a minor impact on the limiting current density of the bioanodes. To more closely investigate the effect of fermentation degree on performance further experiments on shorter time scales (e.g., voltammetric experiments at higher scan rates) would be required.

Among all studied materials, stainless-steel wool EN 1.4113 has shown the most desirable electrochemical behavior, as its limiting current density seems stable at 0.45 ± 0.07 mA·cm^{-2} (1.5 ± 0.2 mA·cm^{-3}) after 4 weeks in an aged medium without significant evidence of corrosion. Over time in chronoamperometry, graphite felt and carbon paper showed a similar performance despite their thickness difference and the polarization curves of both showed a limiting current density of 0.11 ± 0.04 mA·cm^{-2} (0.44 ± 0.16 mA·cm^{-3}) and 0.09 ± 0.05 mA·cm^{-2} (4.3 ± 2.4 mA·cm^{-3}), respectively, in the aged medium. The performance of graphite plate was slightly lower than carbon felt and carbon paper and more sensitive to the changes in media, which conflicts with the criteria for robustness. The poor performance of graphite foil and stainless-steel mesh would classify them as non-ideal for applications in brewery waste water treatment, but probably other parameters related to operational or capital cost might influence the selection of a material for other applications. In general, three-dimensional materials performed better than two-dimensional materials, but the similar performance of carbon felt and carbon paper despite their thickness difference could be an unexpected advantage for the selection and assembling of thinner cells. In this context, the best performing material stainless-steel wool offers the possibility of adjusting its packing density for improved MEC design. In our case we obtained the maximum performance with a packing density of 603 mg·cm^{-3}, but this could be optimized for other applications and operation conditions.

Data availability statement

The original contributions presented in the study are included in the article/Supplementary Material, further inquiries can be directed to the corresponding author.

Author contributions

IV: Conceptualization, methodology, validation, formal analysis, investigation, writing—original draft, writing—review and editing, visualization. SK: Conceptualization, resources, writing—review and editing, supervision, project administration, funding acquisition. OS: Conceptualization, methodology, validation, formal analysis, investigation, data curation, writing—review and editing, supervision.

Funding

The authors gratefully thank the German Ministry of Education and Research (BMBF) for their financial support under the program "BioDME" (Grant No. 02WER1528A).

Acknowledgments

This work contains the valuable contributions of Petra Witte from the Faculty of Geosciences of the University of Bremen for the Scanning Electron Micrographs. Furthermore, the authors thank the group of Prof. Johannes Gescher from the Institute of Technical Microbiology at Hamburg University of Technology for providing the *G. sulfurreducens* PCA strain.

Conflict of interest

The authors declare that the research was conducted in the absence of any commercial or financial relationships that could be construed as a potential conflict of interest.

Publisher's note

Supplementary material

The Supplementary Material for this article can be found online at: https://www.frontiersin.org/articles/10.3389/fenrg.2023.1119090/full#supplementary-material

References

Adachi, M., Yamamoto, R., Shimomura, T., and Miya, A. (2010). Microbial fuel cells with a mediator-polymer modified anode. *Electrochemistry* 78, 814–816. doi:10.5796/ELECTROCHEMISTRY.78.814

Álvarez Esquivel, D. Y., Guo, Y., Brown, R. K., Müller, S., Schröder, U., and Harnisch, F. (2020). Investigating community dynamics and performance during microbial electrochemical degradation of whey. *ChemElectroChem* 7, 989–997. doi:10.1002/celc.201902109

Baudler, A., Langner, M., Rohr, C., Greiner, A., and Schröder, U. (2017). Metal–polymer hybrid architectures as novel anode platform for microbial electrochemical technologies. *ChemSusChem* 10, 253–257. doi:10.1002/cssc.201600814

Baudler, A., Schmidt, I., Langner, M., Greiner, A., and Schröder, U. (2015). Does it have to be carbon? Metal anodes in microbial fuel cells and related bioelectrochemical systems. *Energy Environ. Sci.* 8, 2048–2055. doi:10.1039/c5ee00866b

Bond, D. R., and Lovley, D. R. (2003). Electricity production by Geobacter sulfurreducens attached to electrodes. *Appl. Environ. Microbiol.* 69, 1548–1555. doi:10.1128/AEM.69.3.1548-1555.2003

Coppi, M. V., Leang, C., Sandler, S. J., and Lovley, D. R. (2001). Development of a genetic system for geobacter sulfurreducens. *Appl. Environ. Microbiol.* 67, 3180–3187. doi:10.1128/AEM.67.7.3180-3187.2001

Dhar, B. R., Sim, J., Ryu, H., Ren, H., Santo Domingo, J. W., Chae, J., et al. (2017). Microbial activity influences electrical conductivity of biofilm anode. *Water Res.* 127, 230–238. doi:10.1016/j.watres.2017.10.028

Dumas, C., Mollica, A., Féron, D., Basseguy, R., Etcheverry, L., and Bergel, A. (2008). Checking graphite and stainless anodes with an experimental model of marine microbial fuel cell. *Bioresour. Technol.* 99, 8887–8894. doi:10.1016/j.biortech.2008.04.054

Dumitru, A., and Scott, K. (2016). *Anode materials for microbial Fuel cells*. Elsevier. doi:10.1016/B978-1-78242-375-1.00004-6

Erben, J., Pinder, Z. A., Lüdtke, M. S., and Kerzenmacher, S. (2021). Local acidification limits the current production and biofilm formation of Shewanella oneidensis MR-1 with electrospun anodes. *Front. Microbiol.* 12, 660474. doi:10.3389/fmicb.2021.660474

Fan, X., Zhou, Y., Jin, X., Song, R. Bin, Li, Z., and Zhang, Q. (2021). Carbon material-based anodes in the microbial fuel cells. *Carbon Energy* 3, 449–472. doi:10.1002/cey2.113

Hou, J., Liu, Z., Yang, S., and Zhou, Y. (2014). Three-dimensional macroporous anodes based on stainless steel fiber felt for high-performance microbial fuel cells. *J. Power Sources* 258, 204–209. doi:10.1016/j.jpowsour.2014.02.035

Inoue, K., Qian, X., Morgado, L., Kim, B. C., Mester, T., Izallalen, M., et al. (2010). Purification and characterization of OmcZ, an outer-surface, octaheme c-type cytochrome essential for optimal current production by geobacter sulfurreducens. *Appl. Environ. Microbiol.* 76, 3999–4007. doi:10.1128/AEM.00027-10

Kerzenmacher, S. (2019). Engineering of microbial electrodes. *Adv. Biochem. Eng. Biotechnol.* 167, 135–180. doi:10.1007/10_2017_16

Kipf, E., Erben, J., Zengerle, R., Gescher, J., and Kerzenmacher, S. (2018). Systematic investigation of anode materials for microbial fuel cells with the model organism G. sulfurreducens. *Bioresour. Technol. Rep.* 2, 29–37. doi:10.1016/j.biteb.2018.03.005

Kipf, E., Koch, J., Geiger, B., Erben, J., Richter, K., Gescher, J., et al. (2013). Systematic screening of carbon-based anode materials for microbial fuel cells with Shewanella oneidensis MR-1. *Bioresour. Technol.* 146, 386–392. doi:10.1016/j.biortech.2013.07.076

Kipf, E., Zengerle, R., Gescher, J., and Kerzenmacher, S. (2014). How does the choice of anode material influence electrical performance? A comparison of two microbial fuel cell model organisms. *ChemElectroChem* 1, 1849–1853. doi:10.1002/celc.201402036

Koch, C., Huber, K. J., Bunk, B., Overmann, J., and Harnisch, F. (2019). Trophic networks improve the performance of microbial anodes treating wastewater. *npj Biofilms Microbiomes* 51 (5), 27–29. doi:10.1038/s41522-019-0100-y

Liu, H., Grot, S., and Logan, B. E. (2005). Electrochemically assisted microbial production of hydrogen from acetate. *Environ. Sci. Technol.* 39, 4317–4320. doi:10.1021/es050244p

Madjarov, J., Popat, S. C., Erben, J., Götze, A., Zengerle, R., and Kerzenmacher, S. (2017). Revisiting methods to characterize bioelectrochemical systems: The influence of uncompensated resistance (iR-drop), double layer capacitance, and junction potential. *J. Power Sources* 356, 408–418. doi:10.1016/j.jpowsour.2017.03.033

Pocaznoi, D., Calmet, A., Etcheverry, L., Erable, B., and Bergel, A. (2012). Stainless steel is a promising electrode material for anodes of microbial fuel cells. *Energy Environ. Sci.* 5, 9645–9652. doi:10.1039/c2ee22429a

Riedl, S., Brown, R. K., Alvarez Esquivel, D. Y., Wichmann, H., Huber, K. J., Bunk, B., et al. (2019). Cultivating electrochemically active biofilms at continuously changing electrode potentials. *ChemElectroChem* 6, 2238–2247. doi:10.1002/celc.201900036

Rivera, I., Schröder, U., and Patil, S. A. (2018). *Microbial electrolysis for biohydrogen production: Technical aspects and scale-up experiences*. Elsevier B. doi:10.1016/B978-0-444-64052-9.00036-4

Rousseau, R., Etcheverry, L., Roubaud, E., Basséguy, R., Délia, M. L., and Bergel, A. (2020). Microbial electrolysis cell (MEC): Strengths, weaknesses and research needs from electrochemical engineering standpoint. *Appl. Energy* 257, 113938. doi:10.1016/j.apenergy.2019.113938

Rozendal, R. A., and Buisman, C. J. N. (2005). *Process for producing hydrogen*, 13.

Rozendal, R. A., Hamelers, H. V. M., Euverink, G. J. W., Metz, S. J., and Buisman, C. J. N. (2006). Principle and perspectives of hydrogen production through biocatalyzed electrolysis. *Int. J. Hydrogen Energy* 31, 1632–1640. doi:10.1016/j.ijhydene.2005.12.006

Sonawane, J. M., Patil, S. A., Ghosh, P. C., and Adeloju, S. B. (2018). Low-cost stainless-steel wool anodes modified with polyaniline and polypyrrole for high-performance microbial fuel cells. *J. Power Sources* 379, 103–114. doi:10.1016/j.jpowsour.2018.01.001

Sonawane, J. M., Yadav, A., Ghosh, P. C., and Adeloju, S. B. (2017). Recent advances in the development and utilization of modern anode materials for high performance microbial fuel cells. *Biosens. Bioelectron.* 90, 558–576. doi:10.1016/J.BIOS.2016.10.014

Thauer, R. K., Jungermann, K., and Decker, K. (1977). *Energy conservation in chemotrophic anaerobic bacteria*.

Yaqoob, A. A., Ibrahim, M. N. M., and Guerrero-Barajas, C. (2021). Modern trend of anodes in microbial fuel cells (MFCs): An overview. *Environ. Technol. Innov.* 23, 101579. doi:10.1016/J.ETI.2021.101579